energy&fuels Article
pubs.acs.org/EF

# Influence of Inherent Silicon and Metals in Rice Husk on the Char Properties and Associated Silica Structure

Haiping Yang, Biao Liu, Yingquan Chen,* Bin Li, and Hanping Chen

State Key Laboratory of Coal Combustion, Huazhong University of Science and Technology, 1037 Luoyu Road, Wuhan, Hubei 430074, People's Republic of China

*Supporting Information*

**ABSTRACT:** To obtain high-purity amorphous silica from rice husk char through heat treatment, the distribution of silica and other metallic species in this char and their effects on char combustion reactivity were investigated. The pore properties, crystal structures, and particle sizes of rice husk chars and ashes were analyzed. It was observed that an embedded structure mixing amorphous silica and carbon existed, and its size may be 1−10 nm. This structure may protect the amorphous property of silica during heat treatment. The inherent metallic species were also distributed in the pore size range of 1−10 nm; furthermore, these species accelerated the burnout rate and the crystallization of amorphous silica above 1000 °C.

## 1. INTRODUCTION

Rice husk is an agricultural waste material that is abundantly available in rice-producing countries. Every year, 40 million tons of rice husk is produced worldwide; at present, the combustion of these rice husks is the major disposal method used by grain-processing enterprises, giving rise to considerable pollution of the environment.[1−3] Many industrial boilers have been switching from the use of fossil fuels to rice husk, owing to the high price of fossil fuels that has occurred in China in the last 10 years.[4] The ash generated after burning rice husk has caused severe disposal problems, owing to the presence of crystalline silica (cristobalite form), which is a "Group 1" hazardous compound according to the International Agency for Research on Cancer. The presence of crystalline silica in the ash depends upon the conditions of heat treatment.[5] Therefore, optimization of the heat treatment temperature has the potential to not only benefit the energy output from the organic component in rice husk but also retain silica in an amorphous form as a useful, non-hazardous material. However, there is rarely literature reported on how to obtain energy and high-quality silica simultaneously during thermal conversion of rice husk.

Amorphous silica accounts for 12−20% of the weight of raw rice husk.[6,7] The presence of this silica may discourage various processes involving heat treatment of rice husk, such as combustion and gasification.[8−13] Mansaray and Ghaly[14] previously studied the combustion characteristics of rice husk using thermogravimetric analysis. They found that there were two distinct reaction zones that could be observed for all varieties of rice husk and that the thermal degradation rate in the second reaction zone was significantly lower than that in the first reaction zone, owing to the presence and enrichment of silica in this reaction zone.

Crystallite growth during heat treatment and silica ash production from rice husk has been studied by Ibrahim and Helmy[15] using X-ray diffraction (XRD). It was shown that the nuclei of disordered cristobalite were present in the silica-containing ash, and the nucleation manifested itself at 800−900 °C. The crystallite growth was more pronounced at 1000−1100 °C. Generally, the temperature used during the generation of energy from rice husk is above 800 °C; therefore, little amorphous silica is present in the ash from a high-temperature boiler.[16] The silica distribution in rice husk has been studied by Park et al.[17] using microscopic and microanalytical techniques. Their study showed that most of the silica was present in the outer epidermal cells of rice husk, particularly concentrating in the dome-shaped protrusions.[17] This was determined by examining the silica contents and lignified degree of the outer epidermis, layers of fibers, vascular bundles, parenchyma cells, and inner epidermis of rice husk in sequence from the outer to inner surface. However, the distribution of silica in the rice husk chars undergoing thermal treatment was not found in the literature. In addition, to obtain amorphous silica, temperatures lower than 600 °C were judged to be suitable and used,[18,19] even though such conditions would reduce energy utilization efficiency. It is possible that the silica distribution in rice husk may be protected in its amorphous state and not destroyed during thermal decomposition. To illustrate this possibility, it is necessary to investigate the evolution and distribution of silica in the rice husk char.

There are also other inorganic components, in addition to silica, present in rice husk, such as the metals K, Na, Mg, and Ca. Such inorganic components, especially the metallic species, may influence the characteristics of the resulting amorphous silica. Chandrasekhar et al.[20] compared the characteristics of amorphous silica from raw rice husk and acid-treated rice husk, and the results indicated that an amorphous, reactive, and high-purity silica with high surface area could be prepared from both husks under acid-treating and controlled burning. However, there is no report discussing the reason why acid treatment, which removes all of the metallic species, can enhance the properties of amorphous silica from rice husk.

There are large amounts of micropores in the size range of 0.3−2 nm that are generated during the pyrolysis, gasification, or combustion of rice husk.[21,22] These pores affect the process of burnout of chars. Knudsen diffusion (molecular flow) is the main

**Received:** July 15, 2015
**Revised:** October 19, 2015
**Published:** October 19, 2015

DOI: 10.1021/acs.energyfuels.5b01617
*Energy Fuels* 2015, 29, 7327−7334

Table 1. Contents of Other Inorganic Species (mg/kg, db) in Rice Husk

| samples | K | Na | Ca | Mg | Fe | P | Cl | Al | Si |
|---|---|---|---|---|---|---|---|---|---|
| raw | 4708 | 2280 | 1430 | 899 | 229 | 970 | 6300 | 260 | 58621 |
| acid treated | 37 | 258 | 397 | 351 | 110 | 220 | 320 | 210 | 76785 |

mechanism for mass transfer in these micropores. The equilibrium and kinetics in large pores (>2 nm) are well-described mathematically by traditional methods, such as the Barrett−Joyner−Halenda (BJH) method and the Maxwell−Stefan approach, while the processes within smaller pores (<2 nm) are not suitably described by these traditional methods. The pore size distribution analysis using density functional theory (DFT) was developed well on the characteristics of micro- and mesoporous materials, and especially, its analytical pore size range is from 0.4 to 400 nm, which is stronger than these traditional methods.[23]

In this study, the pore size distribution of rice husk chars with or without silica and the corresponding ash sample were analyzed in detail by the DFT method, to investigate the distribution of amorphous silica in the micro dimension. The distribution of inherent metallic species was also investigated by comparative analysis on the pore size distribution of rice husk chars with or without inherent metallic species. These chars were obtained by pyrolysis of raw or acid-treated rice husk within a range of temperatures from 600 to 1200 °C, which was the major temperature range for thermal conversion of rice husk. Finally, the feasibility to obtain energy and high-quality silica simultaneously during thermal conversion of rice husk was discussed. It is believed that this work is the first report on the discussion of the distribution of amorphous silica and inherent metallic species in the micro dimension and will be useful on rich husk comprehensive utilization.

## 2. MATERIALS AND METHODS

**2.1. Samples.** A rice husk sample from Tuanfeng County in Hubei Province, China, was used in this study. At first, rice husk containing more than 40 wt % moisture was dried at 105 °C. The rice husk was then crushed and sieved to obtain samples with a particle size of 150−300 μm.

The rice husk contained 44.97% C, 7.70% H, 32.46% O, 0.97% N, and 0.07% S on a dry basis (db). Proximate analysis performed on the dry sample indicated a quantity of 69.41% volatile matter and 13.82% ash, resulting in a fixed carbon amount of 16.79%. The lower heating value of the raw rice husk was 14.757 MJ/kg.

To exclude the effect of the other inherent metallic species, such as alkali and alkaline earth metals (AAEM), acid-washing treatment was conducted on the raw rice husk. The rice husk was first treated with 5 M HCl at 55 °C for 30 h and then filtered and washed with a large amount of deionized water until neutralized. After the acid treatment and washing, there was a significant decrease in the AAEM in the rice husk, as shown in Table 1. Figure 1S of the Supporting Information showed the pore size distribution of raw and acid-treated rice husk. In comparison raw rice husk, acid-treated rice husk has a significantly increase of the surface area from 0.16 to 1.23 $m^2/g$, especially the surface area at the pore size from 1 to 10 nm, which has a dramatic increase.

The pyrolysis experiments on the raw and acid-treated samples were carried out in a quartz fixed-bed reactor (35 mm internal diameter), and each experiment consumed about 500 mg of samples. The samples were heated at 10 K $min^{-1}$ from room temperature to the set experimental temperatures (600−1200 °C) and held for about 30 min. A pure $N_2$ flow (99.999%, 100 mL $min^{-1}$) provided the reduction atmosphere. After each trial, the reactor was cooled to room temperature under $N_2$ protection in the furnace. At least five experiments were run under each condition to obtain sufficient chars and to ensure the reproducibility of the experimental data. The repeatability of experiments was very good. The chars from the acid-treated rice husk and the raw rice husk were named AT-*XXX* and R-*XXX* (where "*XXX*" indicates the temperature of the treatment), respectively. The acid-treated rice husk and raw rice husk chars are also referred to as "AT-char" and "R-char", respectively.

To remove the silica, the pyrolysis chars were washed with 20 M concentrated HF at 55 °C for 24 h. As a result of this process, about 99% of the silica was removed. These chars were named "HAT-char" (or HAT-*XXX* when considered alone).

To remove the inherent metallic species of the R-char, acid-washing treatment was also used on the R-chars. These chars were named "ATR-char" (or ATR-*XXX* when considered alone).

After these processes, the resultant chars were ashed at a low temperature (∼500 °C) to obtain the silica. The burning experiment was carried out in a muffle furnace, and each experiment consumed about 200 mg of char lying in the crucible as a thin layer. The samples were heated at 10 K $min^{-1}$ from room temperature to 500 °C and held for more than 5 h to achieve complete burnout. An air flow at 100 mL $min^{-1}$ provided the combustion atmosphere. The ash from the AT-char and R-char were named "AT-ash" and "R-ash", respectively.

**2.2. Characterization of Char and Ash Particles.** Nitrogen isothermal adsorption at −196.15 °C using an automatic adsorption equipment (Micromeritics, ASAP 2020, Norcross, GA) was used to analyze the pore structure characteristics of the chars and ashes. Before the adsorption measurements, the sample was degassed at 150 °C under a vacuum pressure of 30 mmHg for 10 h. To obtain the information pertaining to the micropores, a rather low adsorption pressure was used, with a relative pressure ($P/P_0$) equal to $10^{-7}$, and the $N_2$ adsorption isotherm was obtained at a relative pressure ($P/P_0$) between $10^{-7}$ and 0.995. The specific surface areas and pore size distribution properties were analyzed using the DFT. The calculation process using the DFT was carried out by the ASAP 2020, version 3.01. The reference solid was graphitized thermal carbon black, and the pore model was slit pore. No regularization was used. This approach can be used to calculate the distribution of micro-, meso-, and macropores through a unified method.

The evolution behavior of the crystal structure of the silica in ash obtained from solid char was checked using a powder XRD device (X'Pert PRO, PANalytical B.V., Netherlands) with Cu Kα radiation at $\lambda = 0.154$ nm. The diffraction data were recorded in the $2\theta$ range of 5−105°, with 0.017° step size and 6.35 s step time.

The particle size distribution of the char particles was measured using a Malvern Mastersizer analyzer (Man5004, Malvern, U.K.), which uses the laser diffraction technique and can provide a measurement range from 0.05 to 1000 μm.

The reactivity of the char particles was measured using a thermogravimetric analyzer (TGA, Netzsch STA 409, Germany). Char particles (∼5 mg) were placed in an $Al_2O_3$ crucible, heated to 110 °C, and maintained at that temperature for 10 min to remove the moisture contained in the char particles. The char particles were then heated to 500 °C at a rate of 50 °C/min. The sweeping gas was $N_2$ (99.99%) at a flow rate of 100 mL $min^{-1}$. Then, the purging gas was switched to air at a flow rate of 100 mL $min^{-1}$ for char combustion. The method of thermogravimetric (TG) analysis has been described by Ollero et al.[29] The specific reactivity ($R$) of char at any given time was calculated from the derivative thermogravimetric (DTG) analysis data ($dW/dt$) provided by the thermogravimetry software according to the following equation:

$$R = -\frac{1}{W}\frac{dW}{dt} \tag{1}$$

where $W$ is on the dry and ash-free basis and $R_{50}$, a representative reactivity, was determined from the weighted mean value calculated for the conversion range of 20−80%.

## 3. RESULTS AND DISCUSSION

**3.1. Distribution of Silica in the Rice Husk Chars.** The pore size distribution (in nanometers) of the AT-char obtained using DFT analysis is shown in Figure 1, with the macro-, meso-, and micropore distributions illustrated separately. During pyrolysis, the organic matter was degraded with volatile gas product evolving out, which resulted in many pores on the char surface. As a result, the surface area of AT-600 achieved 351.36 $cm^2/g$, while that of acid-treated rice husk was 1.23 $cm^2/g$. The surface area of the char decreased gradually as the pyrolysis temperature was further increased to 1200 °C. As shown in Figure 1, the surface area of the micropores was quite large, accounting for the main portion of the char surface area. While the surface area of the char decreased when the temperature increased, the major pore size enlarged from 0.5 nm at 600 °C to 1.4 nm at 1200 °C. This might be attributed to dehydrogenation and increase of the aromatic ring size taking place at higher temperatures, thus causing micropores to become larger.

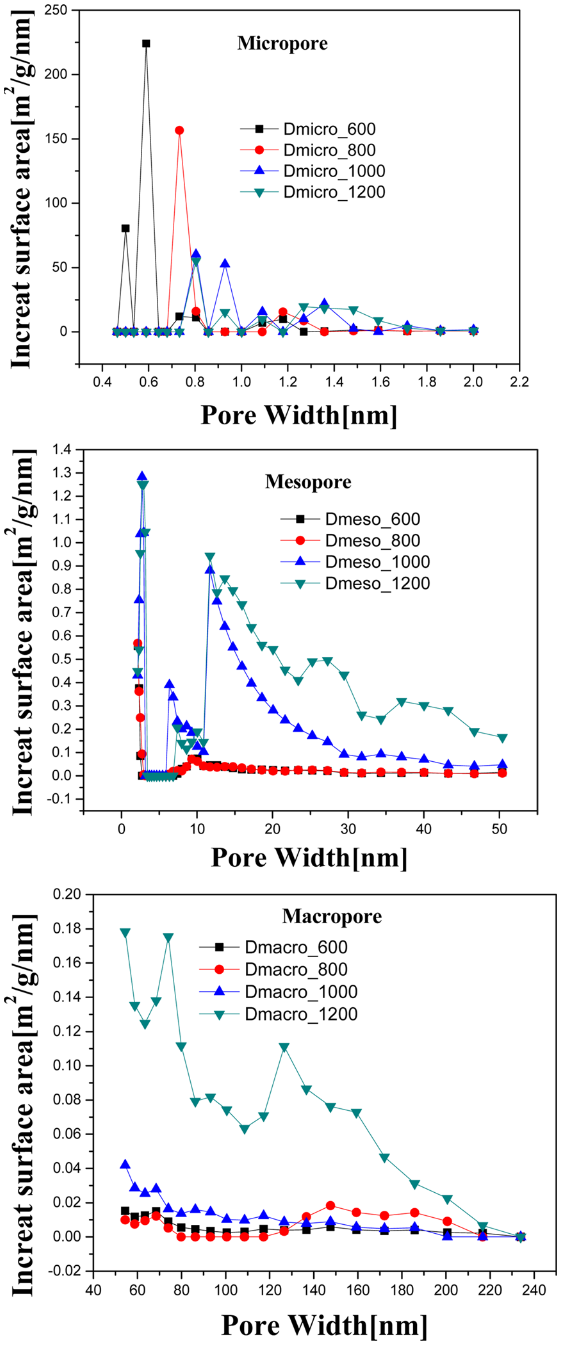

**Figure 1.** Pore size distribution (in nanometers) of AT-chars obtained by DFT analysis: micropore, <2 nm; mesopore, 2−50 nm; and macropore, >50 nm.

The comparison of the surface area between the AT-char and HAT-char obtained by DFT analysis is shown in Figure 2, with

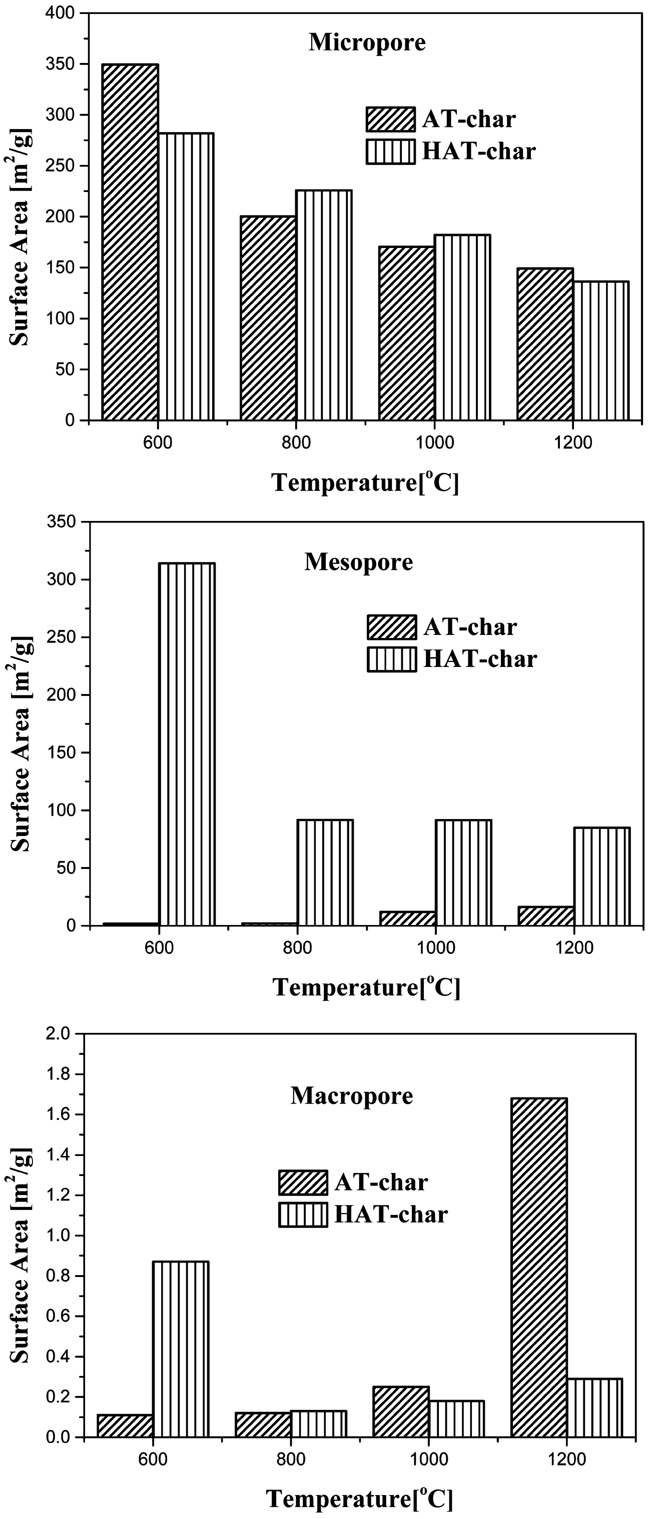

**Figure 2.** Comparison of the surface area between AT-char and HAT-char obtained by DFT analysis: micropore, <2 nm; mesopore, 2−50 nm; and macropore, >50 nm.

the macro-, meso-, and micropore distributions illustrated separately. A significant increase of the surface area was observed after removing silica from the chars. This indicated that removal of silica in the char liberated a large amount of surface area for the pores, which led to a huge pore surface area. The micropores accounted for the major portion of the pore area for the HAT-chars after removal of the silica, but there was also a significant increase in the surface area of the mesopores.

Table 2 shows the median particle size of the AT-series samples (char, ash, and HF-treated char) from the particle size distribution. It can be observed that the size of the HAT-char after removal of silica was much smaller than the AT-char with silica. The particle size distribution of the three types of particles was AT-char > AT-ash > HAT-char, according to the mean diameter data. Consequently, from the pore size distribution analysis and particle size distribution analysis, it can be concluded that there is an embedded structure in the size range of mesopores involving carbon as the continuous phase and silica as inclusions.

**Table 2. Median Particle Size of Char and Ash Particles (in Micrometers)**

| temperature (°C) | AT-char | AT-ash | HAT-char |
|---|---|---|---|
| 600 | 190.51 | 128.99 | 57.81 |
| 800 | 191.23 | 130.26 | 56.32 |
| 1000 | 196.53 | 144.93 | 54.14 |
| 1200 | 195.62 | 143.62 | 54.01 |

**3.2. Distribution of Inherent Metallic Species in the Rice Husk Chars.** The pore size distribution (in nanometers) of the R-chars obtained using DFT analysis is shown in Figure 3, with the macro-, meso-, and micropore distributions illustrated separately. The surface area of the micropores is also the major portion of the total surface area, as was found with the AT-chars, but the total surface areas of the R-chars were smaller than the AT-chars. Increasing the pyrolysis temperature decreased the surface area of the R-chars. The surface area of the R-chars decreased from 82.22 $cm^2/g$ at 600 °C to 33.66 $cm^2/g$ at 1200 °C. The evolution of the surface area between the R-char and ATR-char obtained using DFT analysis is shown in Figure 4, with the macro-, meso-, and micropore distributions illustrated separately. After acid treatment, the inherent metallic species of the R-char were removed and the change of the surface area may be used as the basis for analysis of the distribution of the inherent species. As shown in Figure 4, the surface areas of the macropores of the ATR-chars were similar to those in the R-chars, but there was a significant increase in the scope of the mesopores of the ATR-chars. In addition, there was a considerable increase in the micropore surface area for the ATR-char obtained at 600 °C but little increase for the other three chars obtained above 600 °C. These results indicated that the inherent metallic species were located in the regions of the micro- and mesopores, from which they escaped at high temperatures.

**3.3. Effect of Silicon and Inherent Metallic Species on Combustion Reactivity.** Figure 5 shows the specific reactivity of the chars from the AT-char, HAT-char, and R-char. It is significant that the specific reactivity of the R-char, containing the inherent metallic species, was higher than that of the AT-chars and HAT-chars by a factor of about 10. Generally, a high surface area of char is favorable for the combustion reaction. However, as shown in Figures 2, 4, and 5, the surface area of the R-chars possessing a higher reactivity was lower than that of the AT-chars. This difference can be attributed to the catalytic effect of the inherent metallic species.

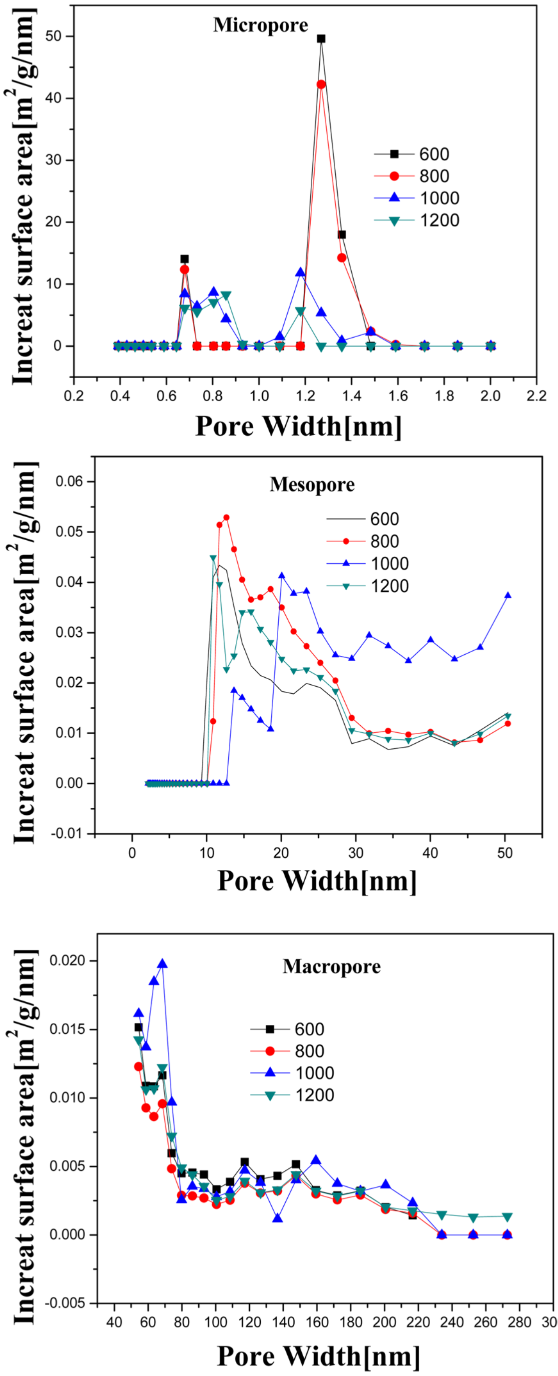

**Figure 3.** Pore size distribution (in nanometers) of R-chars obtained by DFT analysis: micropore, <2 nm; mesopore, 2−50 nm; and macropore, >50 nm.

The specific reactivity of the HAT-chars was a little higher than that of the AT-chars. The relationship between $R_{50}$ and surface area is shown in Figure 6. For the AT-chars, the reaction between carbon and oxygen may be on the micropore surfaces based on the good linear relationship of $R_{50}$ and micropore surface area, which was evident by the research on the coal combustion.[24] However, for the HAT-char, there was a good linear relationship between $R_{50}$ and total surface area, illustrating that the reaction between carbon and oxygen could involve all of the pores. Half of the weight of the AT-char was taken up by silica, which may be

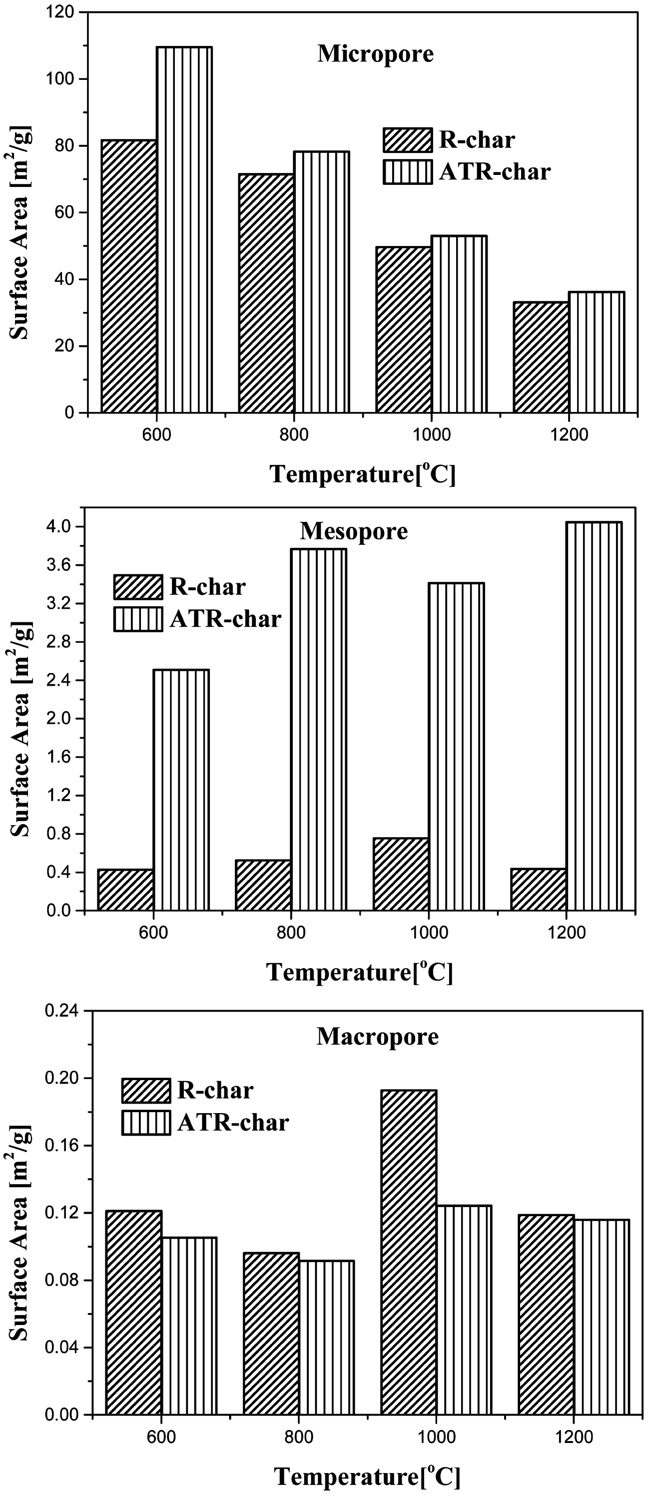

**Figure 4.** Comparison of the surface area between R-char and ATR-char obtained by DFT analysis: micropore, <2 nm; mesopore, 2−50 nm; and macropore, >50 nm.

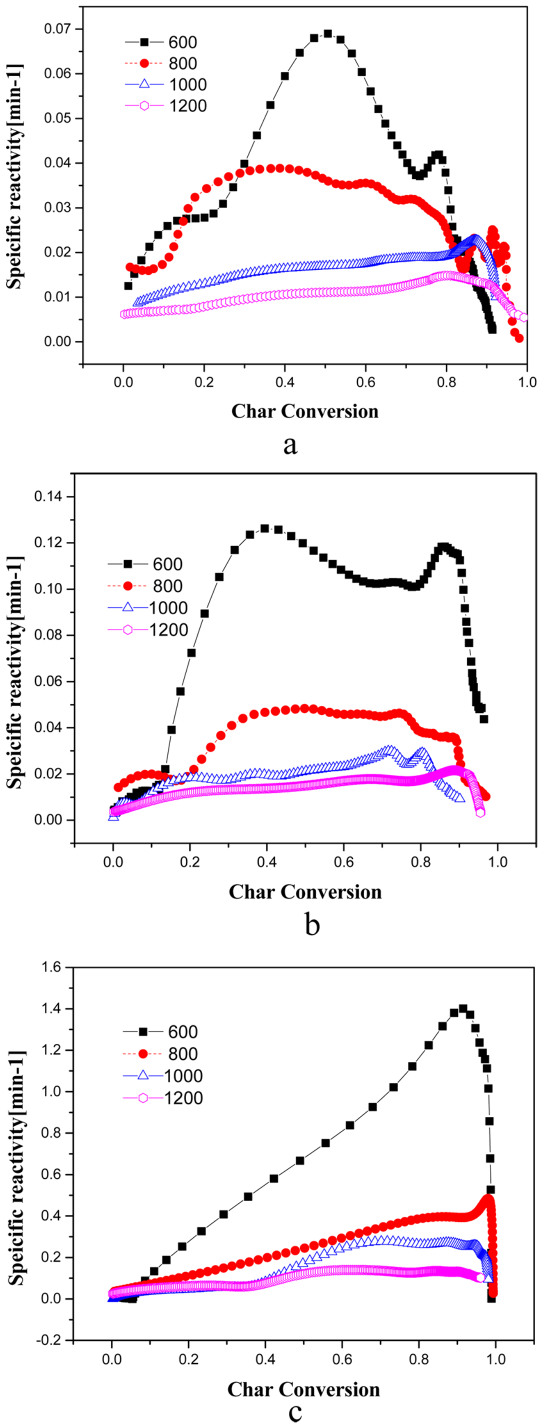

**Figure 5.** Specific reactivities of the chars measured in air in TGA at 450 °C: (a) AT-char, (b) HAT-char, and (c) R-char.

non-active. There was no good linear relationship between $R_{50}$ and surface area for the R-char, likely owing to the presence of inherent metallic species that could have a catalytic effect on the gas−solid reaction.[25,26]

**3.4. Properties of the Ash.** The evolution of pore size distribution of the AT-ashes is shown in Figure 7. It was observed that, for all ash, there were nearly no micropores less than 1 nm. The major pores exhibited a range of 1−10 nm, accounting for 90% of all of the area. In comparison of the results of Figures 1, 3, and 8, it was observed that the argument of the pore surface area increasing with the removal of silica from chars was nearly equal to the pore surface area of ash samples that only contained silica. This proved that the assumption of an embedded structure of silica existing in the char was correct.

The evolution of the pore size distribution of the R-ash samples is shown in Figure 8. The evolution of the pore size distribution of the R-ashes was similar to that of the AT-ash samples, except for a lower surface area resulting from the inherent metallic species.

DOI: 10.1021/acs.energyfuels.5b01617
*Energy Fuels* 2015, 29, 7327−7334

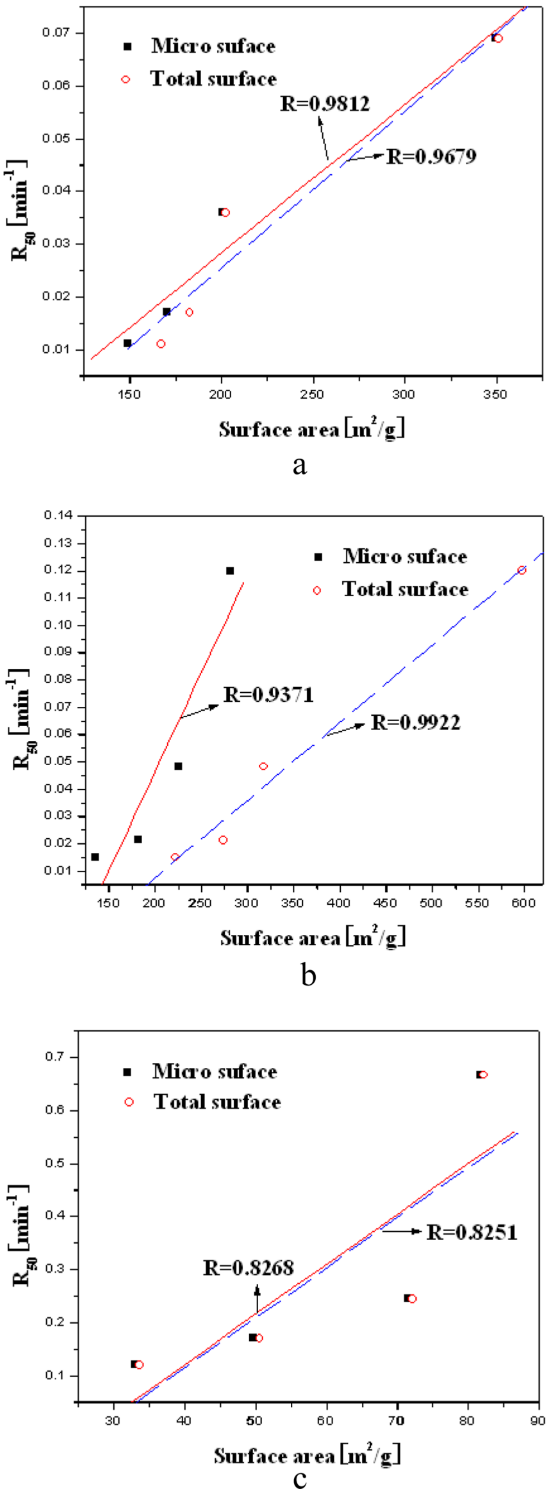

**Figure 6.** Relationship between $R_{50}$ and surface area: (a) AT-char, (b) HAT-char, and (c) R-char.

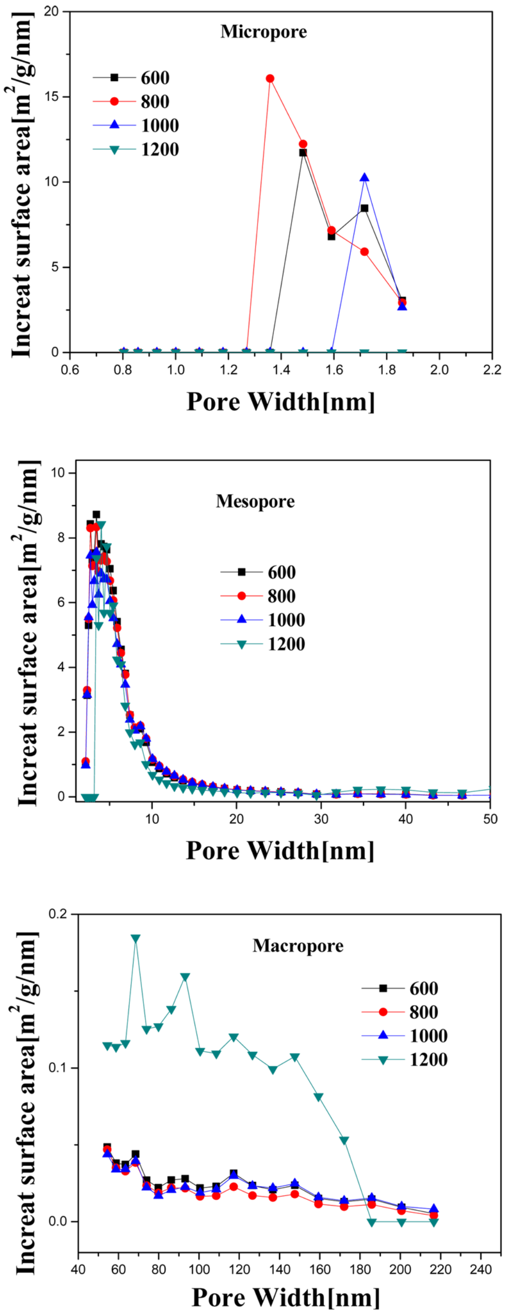

**Figure 7.** Pore size distribution (in nanometers) of AT-ashes obtained by DFT analysis: micropore, <2 nm; mesopore, 2−50 nm; and macropore, >50 nm.

According the results of the XRD analysis of the AT-ash and R-ash shown in Figures 9 for the AT-ash samples, as the temperature increased, the disorder of the amorphous silica decreased, crystallinity enhanced, and tridymite appeared when the temperature reached 1200 °C. However, there was still about 30% of amorphous silica in the ash from the char at 1200 °C. It is suggested that the embedded structure of the silica inclusions in a continuous phase of carbon could protect the amorphous nature of silica. For the R-ash samples, tridymite appeared when the temperature was above 1000 °C and may be attributed to the high reactivity of the inherent metallic species.

As mentioned above, it is probable that the embedded structure between the carbon basis and silica may protect the amorphous property of silica during heat treatment. A thermal conversion roadmap of the processes used on the rice husk to obtain energy and high-quality silica simultaneously is shown in Figure 10. To prevent crystallization of silica, a suitable ratio of carbon and silica in the thermal-treated product of rice husk is needed and a thermal treatment temperature and conversion reactor should be appropriate. Generally, a fixed bed is used to combust rice husk to obtain the heat needed, but the temperature at burning may be up to above 1100 °C; therefore, it is difficult to produce high-quality silica from rice husk ash. Thus, to generate

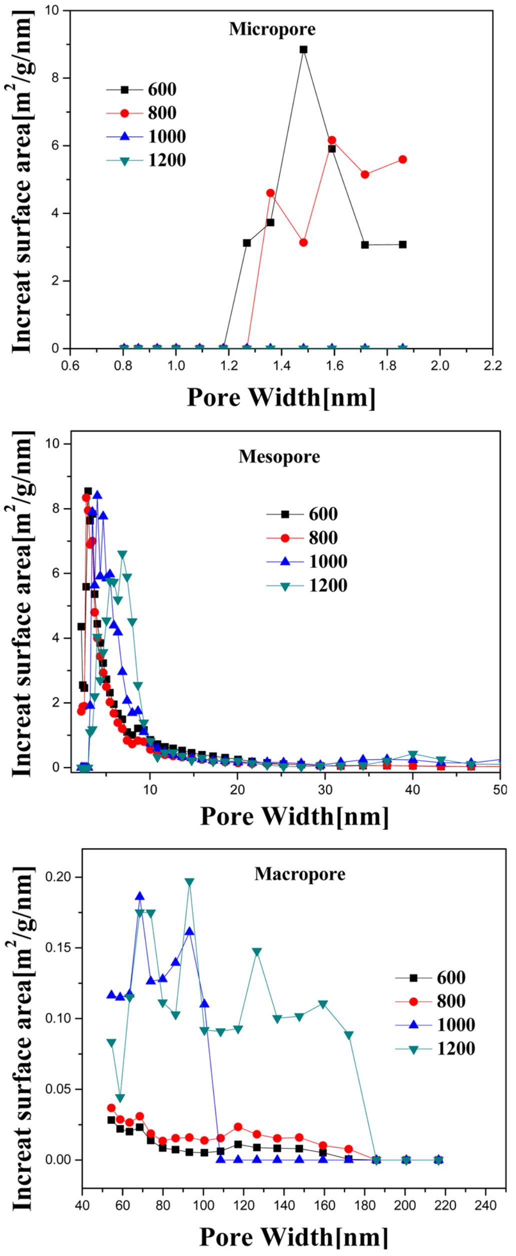

**Figure 8.** Pore size distribution (in nanometers) of R-ashes obtained by DFT analysis: micropore, <2 nm; mesopore, 2−50 nm; and macropore, >50 nm.

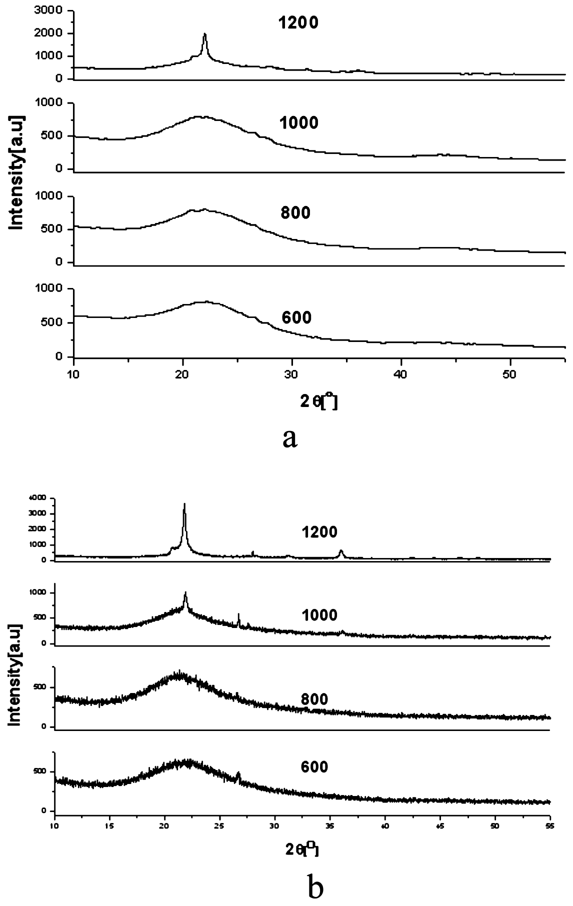

**Figure 9.** XRD pattern of (a) AT-ashes and (b) R-ash samples.

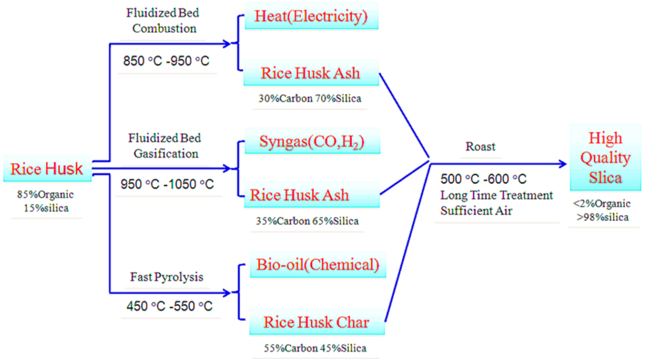

**Figure 10.** Thermal conversion roadmap of rice husk to obtain the energy and high-quality silica simultaneously.

the heat needed for the combustion of rice husk, a fluidized bed, whose operation temperature can be easily retained at 850−950 °C when the crystallization of silica has not begun, is recommended. Furthermore, the operation for the burnout of rice husk is not used to retain about 30 wt %[27] of carbon in the rice husk ash. A syngas from the gasification of rice husk can also be obtained, and use of a gasification reactor derived from a fluidized bed is also recommended for this process. The gasification temperature may be up to 1050 °C, and the content of carbon in the rice husk ash may be up to about 35%[28] to protect the embedding structure. A moderate thermal treatment, fast pyrolysis at 450−550 °C, may be more suitable to obtain energy and silica simultaneously, but the rice husk char generated during pyrolysis has a high carbon content (up to 55 wt %), which means that more energy is wasted. However, the rice husk ash from combustion and gasification of the rice husk char is not directly used as silica because of its relatively high carbon content. Therefore, a moderate and long roast time at 500−600 °C should be used to obtain high-quality silica, in which the content of carbon is below 2 wt %.

## 4. CONCLUSION

The experimental data in this study showed that a large number of pores were generated during pyrolysis of rice husk in the temperature range of 600−1200 °C. After removal of silica from the char, the pores sizes increased 1−10 nm. Most of the pores in the ash obtained from the same char were in the range of 1−10 nm, which indicates that an embedded structure having a size range of 1−10 nm existed between the continuous phase of carbon and inclusions of silica. Such a structure may protect the amorphous nature of the silica during heat treatment. The inherent metallic species were also distributed in the range of pores from 1 to 10 nm. Furthermore, these species accelerated the burnout rate and the crystallization of amorphous silica above 1000 °C.

## ■ ASSOCIATED CONTENT

### Ⓢ Supporting Information

The Supporting Information is available free of charge on the ACS Publications website at DOI: 10.1021/acs.energyfuels.5b01617.

> Pore size distribution of raw rice husk and acid-treated rice husk by DFT (Figure 1S) and TGA curve for combustion of raw rice husk and acid-treated rice husk (Figure 2S) (PDF)

## ■ AUTHOR INFORMATION

### Corresponding Author

*E-mail: chenyingquan@hust.edu.cn.

### Notes

The authors declare no competing financial interest.

## ■ ACKNOWLEDGMENTS

The authors express great appreciation for the financial support from the Special Fund for Agro-scientific Research in the Public Interest (201303095), the Key Projects of National Fundamental Research Planning (2013CB228102), and the National Natural Science Foundation of China (51376076 and 51306067). The authors are also grateful for the technical support from the Analytical and Testing Center at the Huazhong University of Science and Technology (http://atc.hust.edu.cn).

## ■ REFERENCES

(1) Hongo, T.; Sugiyama, J.; Yamazaki, A.; Yamasaki, A. Synthesis of imogolite from rice husk ash and evaluation of its acetaldehyde adsorption ability. *Ind. Eng. Chem. Res.* **2013**, *52* (5), 2111−2115.

(2) Jingjing, L.; Xing, Z.; DeLaquil, P.; Larson, E. D. Biomass energy in China and its potential. *Energy Sustainable Dev.* **2001**, *5* (4), 66−80.

(3) Liu, H.; Jiang, G. M.; Zhuang, H. Y.; Wang, K. J. Distribution, utilization structure and potential of biomass resources in rural China: With special references of crop residues. *Renewable Sustainable Energy Rev.* **2008**, *12* (5), 1402−1418.

(4) Wu, C. Z.; Yin, X. L.; Yuan, Z. H.; Zhou, Z. Q.; Zhuang, X. S. The development of bioenergy technology in China. *Energy* **2010**, *35* (11), 4445−4450.

(5) Bhagiyalakshmi, M.; Yun, L. J.; Anuradha, R.; Jang, H. T. Utilization of rice husk ash as silica source for the synthesis of mesoporous silicas and their application to $CO_2$ adsorption through TREN/TEPA grafting. *J. Hazard. Mater.* **2010**, *175* (1−3), 928−938.

(6) Lin, L.; Zhai, S. R.; Xiao, Z. Y.; Liu, N.; Song, Y.; Zhai, B.; An, Q. D. Cooperative effect of polyethylene glycol and lignin on $SiO_2$ microsphere production from rice husks. *Bioresour. Technol.* **2012**, *125* (0), 172−174.

(7) Zhang, H.; Zhao, X.; Ding, X.; Lei, H.; Chen, X.; An, D.; Li, Y.; Wang, Z. A study on the consecutive preparation of d-xylose and pure superfine silica from rice husk. *Bioresour. Technol.* **2010**, *101* (4), 1263−1267.

(8) Bhat, A.; Ram Bheemarasetti, J. V.; Rajeswara Rao, T. Kinetics of rice husk char gasification. *Energy Convers. Manage.* **2001**, *42* (18), 2061−2069.

(9) Demirbas, A. Potential applications of renewable energy sources, biomass combustion problems in boiler power systems and combustion related environmental issues. *Prog. Energy Combust. Sci.* **2005**, *31* (2), 171−192.

(10) Zhao, Y.; Sun, S.; Tian, H.; Qian, J.; Su, F.; Ling, F. Characteristics of rice husk gasification in an entrained flow reactor. *Bioresour. Technol.* **2009**, *100* (23), 6040−6044.

(11) Li, D.; Chen, D.; Zhu, X. Reduction in time required for synthesis of high specific surface area silica from pyrolyzed rice husk by precipitation at low pH. *Bioresour. Technol.* **2011**, *102* (13), 7001−7003.

(12) Kalapathy, U.; Proctor, A.; Shultz, J. An improved method for production of silica from rice hull ash. *Bioresour. Technol.* **2002**, *85* (3), 285−289.

(13) Kalapathy, U.; Proctor, A.; Shultz, J. A simple method for production of pure silica from rice hull ash. *Bioresour. Technol.* **2000**, *73* (3), 257−262.

(14) Mansaray, K. G.; Ghaly, A. E. Determination of kinetic parameters of rice husks in oxygen using thermogravimetric analysis. *Biomass Bioenergy* **1999**, *17* (1), 19−31.

(15) Ibrahim, D. M.; Helmy, M. Crystallite growth of rice husk ash silica. *Thermochim. Acta* **1981**, *45* (1), 79−85.

(16) Chareonpanich, M.; Jullaphan, O.; Tang, C. Bench-scale synthesis of zeolite A from subbituminous coal ashes with high crystalline silica content. *J. Cleaner Prod.* **2011**, *19* (1), 58−63.

(17) Park, B. D.; Wi, S. G.; Lee, K. H.; Singh, A. P.; Yoon, T. H.; Kim, Y. S. Characterization of anatomical features and silica distribution in rice husk using microscopic and micro-analytical techniques. *Biomass Bioenergy* **2003**, *25* (3), 319−327.

(18) James, J.; Rao, M. S. Silica from rice husk through thermal decomposition. *Thermochim. Acta* **1986**, *97* (0), 329−336.

(19) Ahmed, Y. M. Z.; Ewais, E. M.; Zaki, Z. I. Production of porous silica by the combustion of rice husk ash for tundish lining. *J. Univ. Sci. Technol. Beijing* **2008**, *15* (3), 307−313.

(20) Chandrasekhar, S.; Pramada, P. N.; Praveen, L. Effect of organic acid treatment on the properties of rice husk silica. *J. Mater. Sci.* **2005**, *40* (24), 6535−6544.

(21) Fu, P.; Hu, S.; Sun, L.; Xiang, J.; Yang, T.; Zhang, A.; Zhang, J. Structural evolution of maize stalk/char particles during pyrolysis. *Bioresour. Technol.* **2009**, *100* (20), 4877−4883.

(22) Hu, S.; Xiang, J.; Sun, L.; Xu, M.; Qiu, J.; Fu, P. Characterization of char from rapid pyrolysis of rice husk. *Fuel Process. Technol.* **2008**, *89* (11), 1096−1105.

(23) Do, D. D.; Do, H. D. Pore Characterization of Carbonaceous Materials by DFT and GCMC Simulations: A Review. *Adsorpt. Sci. Technol.* **2003**, *21* (5), 389−423.

(24) Dudzinska, A. The Effect of Pore Volume of hard coals on their susceptibility to spontaneous combustion. *J. Chem.* **2014**, *2014*, 1−7.

(25) Kitsuka, T.; Bayarsaikhan, B.; Sonoyama, N.; Hosokai, S.; Li, C. Z.; Norinaga, K.; Hayashi, J. Behavior of inherent metallic species as a crucial factor for kinetics of steam gasification of char from coal pyrolysis. *Energy Fuels* **2007**, *21* (2), 387−394.

(26) Yip, K.; Tian, F. J.; Hayashi, J.; Wu, H. W. Effect of alkali and alkaline earth metallic species on biochar reactivity and syngas compositions during steam gasification. *Energy Fuels* **2010**, *24*, 173−181.

(27) Han-ping, C.; Bin, L.; Hai-ping, Y.; Xian-hua, W.; Shi-hong, Z. Status and prospect of biomass combustion technology. *Ind. Boiler* **2009**, *12* (5), 1−7.

(28) Shihong, Z.; Xiangpeng, L.; Guangchang, H.; Haiping, Y.; Xianhua, W.; Hanping, C. Gasification property of agriculture wastes in an updraft fixed bed gasifier with top-lit ignition. *Trans. Chin. Soc. Agric. Eng.* **2013**, *29* (10), 196−202.

(29) Ollero, P.; Serrera, A.; Arjona, R.; Alcantarilla, S. The $CO_2$ gasification kinetics of olive residue. *Biomass Bioenergy* **2003**, *24*, 151−161.